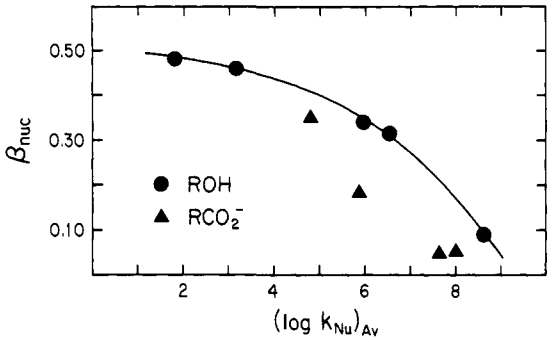

Figure 7. A plot of β_{nuc} for the reactions of alkyl alcohols (●) and carboxylate ions (▲) with $XArCH(CF_3)^+$ against log $(k_{Nu})_{av}$, the arithmetic average of the largest and smallest rate constants of the respective Brønsted correlations.

an electron pair at the nucleophile for reaction with the carbocation. Therefore, β_d will be negative for strongly solvated nucleophiles because increasing the basicity of the nucleophile will lead to a decrease in K_d, due to an increase in the strength of the solvent–nucleophile hydrogen bond.[50] The following show that $\beta_d < 0$ for the addition of amines to carbocations, so that $(\beta_{nuc})_{obsd} = 0.29$ for the addition of amines to $4\text{-}Me_2NArCH(CF_3)^+$ must be substantially smaller than $(\beta_{nuc})_c$ (eq 3).

(1) The value of $(\beta_{nuc})_{obsd} = -0.08$ for the reaction of amine nucleophiles with $4\text{-}MeSArCH(CF_3)^+$ requires $\beta_d < 0$. The reactions of amines with $4\text{-}MeSArCH(CF_3)^+$ are limited by the rate of conversion of the solvated amine to the amine–carbocation contact ion–dipole pair (k_d, Scheme II).[37]

(2) McClelland, Steenken, and co-workers have studied the reactions of amine nucleophiles with ring-substituted diaryl- and triarylmethyl carbocations. The data for these reactions can be fit to Scheme II using a value of $\beta_d = -0.2$.[10]

The limiting rate constant for the reaction of acetate ion with ring-substituted 1-phenylethyl carbocations is $k_{AcO} = 5 \times 10^8\ M^{-1}\ s^{-1}$.[11] This is 10-fold slower than that expected for a diffusion-controlled reaction. Therefore, the rate of these reactions is limited by some step other than diffusional encounter, which probably corresponds to cleavage of a carboxylate–solvent hydrogen bond.[11]

Figure 7 shows a plot of β_{nuc} against $(\log k_{Nu})_{av}$ for the reactions of carboxylate ions and alkyl alcohols with $XArCH(CF_3)^+$, where $(\log k_{Nu})_{av}$ is the arithmetic average of the largest and smallest values of $\log k_{Nu}$ for the respective Brønsted correlations. This plot shows that the selectivity for the reactions of carboxylate ions is lower than that for the reactions of alcohols of the same reactivity. This difference in $(\beta_{nuc})_{obsd}$ for carboxylate ions and alcohols is probably due, at least in part, to a more negative value of β_d for the more strongly solvated carboxylate ions.

Acknowledgment. We acknowledge National Institute of General Medical Sciences Grant GM 39754 for support of this work.

(50) Jencks, W. P.; Haber, M. T.; Herschlag, D.; Nazaretian, K. *J. Am. Chem. Soc.* **1986**, *108*, 479–483. Berg, U.; Jencks, W. P. *J. Am. Chem. Soc.* **1991**, *113*, 6997–7002.

(51) Richard, J. P.; Amyes, T. L.; Vontor, T. *J. Am. Chem. Soc.* **1991**, *113*, 5871–5873.

Effects of Dehydroalanine on Peptide Conformations

Darryl Erik Palmer,[†] Christian Pattaroni,[†] Kenichi Nunami,[†] Raj K. Chadha,[†] Murray Goodman,*[,†] Tateaki Wakamiya,[‡] Koichi Fukase,[‡] Shingo Horimoto,[‡] Manabu Kitazawa,[‡] Hiroshi Fujita,[‡] Akira Kubo,[‡] and Tetsuo Shiba[‡]

Contribution from the University of California at San Diego, La Jolla, California 92093-0343, and Osaka University, Toyonaka, Osaka 560, Japan. *Received February 10, 1992*

Abstract: The conformational preferences of dehydroalanine were examined through a combined approach of X-ray diffraction, NMR spectroscopy, and molecular modeling. Monte Carlo simulated annealing was used in conjunction with X-ray diffraction data and semiempirical quantum mechanical calculations to determine appropriate parameters for modeling dehydroalanine with the DISCOVER consistent valence force field. The two molecules in the asymmetric unit of *N*-acetyldehydroalanine *N'*-methylamide were simulated in the crystalline environment using these optimized parameters. The rms deviations between simulation and experimental data for heavy atom bond lengths, bond angles, and torsions were 0.021 Å, 1.9°, and 8.7°, respectively. The dehydroalanine-containing ring A fragment of nisin and two analogs with either L- or D-alanine substituted for dehydroalanine were synthesized and examined by NMR spectroscopy. Using distance geometry followed by conformational energy minimization with our optimized parameters, families of conformations were determined for each molecule which satisfied the observed backbone NOE, $J_{\alpha N}$ coupling constants, and temperature coefficients. Dehydroalanine adopted a roughly planar conformation, with trans orientations for the ϕ and ψ torsions, and induced an inverse γ-turn in the preceding residue. Similar effects have been observed for linear, dehydroalanine-containing peptides in solution and as crystals, suggesting that dehydroalanine exerts a powerful conformational influence independent of other constraints. The conformational preferences of the L- and D-Ala ring A analogs differed substantially from each other and from the ring A fragment.

Introduction

Dehydroalanine (Dha) is an α,β-unsaturated amino acid which plays a catalytic role in the active sites of some yeast[1] and bacterial[2] enzymes. It also occurs in a variety of peptide antibiotics of bacterial origin, including the "lantibiotics" nisin,[3] subtilin,[4] epidermin,[5] and gallidermin,[6] and more highly modified peptides

* Correspondence should be addressed to Professor Murray Goodman, University of California at San Diego, Department of Chemistry, 9500 Gilman Dr., La Jolla, CA 92093-0343.

[†] University of California at San Diego.

[‡] Osaka University.

(1) Parkhurst, J. R.; Hodgins, D. S. *Arch. Biochem. Biophys.* **1972**, *152*, 597–605.

(2) Wickner, R. B. *J. Biol. Chem.* **1969**, *244*, 6550–6552.

(3) Gross, E.; Morell, J. *J. Am. Chem. Soc.* **1967**, *89*, 2791–2792.

(4) Gross, E.; Morell, J. L.; Craig, L. C. *Proc. Natl. Acad. Sci. U.S.A.* **1969**, *62*, 952–956.

(5) Allgaier, H.; Jung, G.; Werner, R. G.; Schneider, U.; Zähner, H. *Angew. Chem., Int. Ed. Engl.* **1985**, *24*, 1051–1053.

0002-7863/92/1514-5634$03.00/0

Scheme I

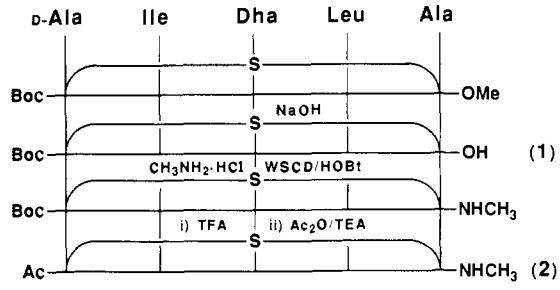

such as thiostrepton, siomycin-A,[7] nosiheptide,[8] and berninamycin.[9] Novel active antibiotics[10] and immuno-adjuvants[11] have been synthesized by substituting dehydroalanine for other residues.

Biosynthetically, the dehydroalanine in the lantibiotics originates from the dehydration of serine residues.[12-14] The subsequent stereospecific intramolecular addition of thiols from cysteines generates the *meso*-lanthionine bridges which give the lantibiotics their name. The remaining dehydroalanines are important for biological activity,[15,16] although it is still unclear whether this is a conformational effect or is due to the chemical reactivity of the group.[17]

The structural preferences of dehydroalanine-containing peptides and model compounds previously have been investigated by X-ray crystallography[18,19] and NMR,[20-22] UV,[23] and IR[22] spectroscopy. In all cases, a nearly planar conformation was determined. The NMR spectroscopy and X-ray crystallography consistently revealed a trans orientation of the ϕ and ψ torsions. One group has reported parameters for modeling α,β-unsaturated amino acids with an empirical potential energy function; however, their calculations predict that the energetically most favorable conformation has trans and cis orientations of the ϕ and ψ torsions, respectively.[24]

In our work, we have employed synthesis, X-ray diffraction, semiempirical quantum mechanical calculations, and simulated annealing to derive suitable parameters for modeling dehydroalanine with the DISCOVER consistent valence force field (CVFF).[25] We then used DISCOVER, along with NMR and distance geometry calculations, to characterize the profound conformational effects of replacing dehydroalanine with L- or D-alanine in the ring A fragment of nisin.

Scheme II

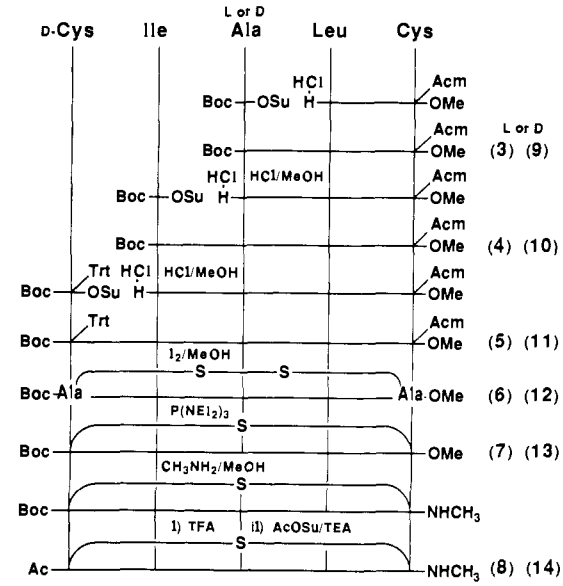

Methods

Synthesis. All melting points are uncorrected. The FD-MS spectra were obtained with a JEOL JMS-DX 300 mass spectrometer. Specific rotations were obtained with a Perkin-Elmer 141 polarimeter. HPLC was carried out with a Shimadzu LC-5A or 6A liquid chromatograph. Amino acid analysis was carried out with a Hitachi 655A type liquid chromatograph system equipped with a 655-3410 unit (column, Hitachi custom #2619F, 4 × 150 mm, 58 °C; buffer, sodium citrate;[26] flow rate, 0.4 mL/min). Samples for amino acid analysis were hydrolyzed with constant boiling 6 M HCl in sealed tubes at 110 °C for 40 h.

The abbreviations used are as follows: Acm, acetamidomethyl; Ala_L, alanyl portion of lanthionine; Boc, *tert*-butyloxycarbonyl; Dha, dehydroalanine; Dhb, α-amino-α,β-dehydrobutyric acid residue; DMF, *N,N*-dimethylformamide; DMSO, dimethyl sulfoxide; EDC, 1-ethyl-3-[3-(dimethylamino)propyl]carbodiimide; Lan, lanthionine; Trt, trityl; LB, exponential line broadening factor; AT, acquisition time.

Boc-D-Ala_L-Ile-Dha-Leu-Ala_L-OH (1). To a solution of Boc-D-Ala_L-Ile-Dha-Leu-Ala_L-OMe[27] (400 mg, 0.667 mmol) in dioxane (12 mL) was added a 1 M NaOH solution (734 μL, 0.734 mmol). After the solution was stirred at 10 °C overnight, 10% aqueous citric acid solution and EtOAc were added to the solution. The organic layer was washed with 10% aqueous citric acid and saturated NaCl solution, dried over $MgSO_4$, and then concentrated under reduced pressure. The residue was purified by silica gel column chromatography (Merck silica gel 60 (230–400 mesh), 25 g, 2 × 28 cm, $CHCl_3$:MeOH:AcOH = 30:2:1) to give **1**, which was precipitated from $CHCl_3$ and hexane: yield, 216 mg (55.2%); mp 214–218 °C; $[\alpha]^{21}_D$ −63.8° (*c* 0.32, MeOH). Anal. Calcd for $C_{26}H_{43}O_8N_5S\cdot0.5H_2O$: C, 52.51; H, 7.46; N, 11.78; S, 5.39. Found: C, 52.83; H, 7.42; N, 11.81; S, 4.90.

Ac-D-Ala_L-Ile-Dha-Leu-Ala_L-$NHCH_3$ (2). To a solution of **1** (70.0 mg, 0.120 mmol), methylamine hydrochloride (8.9 mg, 0.132 mmol), and

(6) Kellner, R.; Jung, G.; Hörner, T.; Zähner, H.; Schnell, N.; Entian, K.-D.; Götz, F. *Eur. J. Biochem.* **1988**, *177*, 53–59.
(7) Tori, K.; Tokura, K.; Okabe, K.; Ebata, M.; Otsuka, H. *Tetrahedron Lett.* **1976**, *3*, 185–188.
(8) Pascard, C.; Ducruix, A.; Lunel, J.; Prangé, T. *J. Am. Chem. Soc.* **1977**, *99*, 6418–6423.
(9) Pearce, C. J.; Rinehart, K. L., Jr. *J. Am. Chem. Soc.* **1979**, *101*, 5069–570.
(10) Ando, S.; Kato, T.; Izumiya, N. *Int. J. Pept. Protein Res.* **1985**, *25*, 15–26.
(11) Kundu, B.; Rizvi, S. Y.; Haq, W.; Saxena, R. P.; Saxena, K. C.; Mathru, K. B. *Indian J. Biochem. Biophys.* **1987**, *24*, 129–132.
(12) Schnell, N.; Entian, K.-D.; Schneider, U.; Götz, F.; Zähner, H.; Kellner, R.; Jung, G. *Nature* **1988**, *333*, 276–278.
(13) Banerjee, S.; Hansen, J. N. *J. Biol. Chem.* **1988**, *263*, 9508–9514.
(14) Buchman, G. W.; Banerjee, S.; Hansen, J. N. *J. Biol. Chem.* **1988**, *263*, 16260–16266.
(15) Chan, W. C.; Bycroft, B. W.; Lian, L.-Y.; Roberts, G. C. K. *FEBS Lett.* **1989**, *252*, 29–36.
(16) Wakamiya, T.; Tukase, K.; Kitazawa, M.; Fujita, H.; Kubo, A.; Maeshiro, Y.; Shiba, T. In *Peptides: Chemistry, Structure and Biology (Proc. Eleventh Am. Pept. Symp.)*; Rivier, J. E., Marshall, G. R., Eds.; ESCOM: Leiden, 1990; p 60–64.
(17) Morris, S. L.; Walsh, R. C.; Hansen, J. N. *J. Biol. Chem.* **1984**, *259*, 13590–4.
(18) Ajò, D.; Granozzi, G.; Tondello, E.; Del Prà, A.; Zanotti, G. *J. Chem. Soc., Perkin Trans. 2* **1979**, 927–929.
(19) Anderson, B.; Hodgkin, D. C.; Viswamitra, M. A. *Nature* **1970**, *225*, 233–235.
(20) Freund, S.; Jung, G.; Gutbrod, O.; Folkers, G.; Gibbons, W. A.; Allgaier, H.; Werner, R. *Biopolymers* **1991**, *31*, 803–811.
(21) Tori, K.; Tokura, K.; Yoshimura, Y.; Okabe, K.; Otsuka, H.; Inagaki, F.; Miyazawa, T. M. *J. Antibiot.* **1979**, *32*, 1072–1077.
(22) Gupta, A.; Chauhan, V. S. *Biopolymers* **1990**, *30*, 395–403.
(23) Mayoral, J. C.; Cativiela, C.; Lopez, M. P.; Ajò, D.; De Zuane, F. *J. Crystallogr. Spectrosc. Res.* **1989**, *19*, 993–1001.
(24) Ajò, D.; Granozzi, G.; Tondello, E.; Del Prà, A. *Biopolymers* **1980**, *19*, 469–475.
(25) Dauber-Osguthorpe, P.; Roberts, V. A.; Osguthorpe, D. J.; Wolff, J.; Genest, M.; Hagler, A. T. *Proteins: Struct. Funct. Genet.* **1988**, *4*, 31–47.
(26) The buffer system was slightly different from the standard system in order to separate *meso*-lanthionine and methyllanthionine from other amino acids: buffer A, sodium citrate dihydrate 7.34 g, NaCl 5.02 g, citric acid monohydrate 20.56 g, EtOH 104 mL, 2,2′-thiobisethanol 5.22 mL, and octanoic acid 0.1 mL in 1000 mL of aqueous solution; buffer B, sodium citrate dihydrate 26.67 g, NaCl 54.35 g, citric acid monohydrate 6.10 g, EtOH 40 mL, and octanoic acid 0.1 mL in 1000 mL of aqueous solution. Gradient: A 100% (0–12 min), A 85% (12–37 min), A 19%/B 81% (37–47 min), B 100% (47–62 min).
(27) Wakamiya, T.; Shimbo, K.; Sano, A.; Fukase, K.; Shiba, T. *Bull. Chem. Soc. Jpn.* **1983**, *56*, 2044–2049.

HOBt (16.2 mg, 0.120 mmol) in DMF (2 mL) was added EDC (20.5 mg, 0.132 mmol) at −70 °C. After the solution was stirred at −20 °C overnight, 10% aqueous citric acid solution and EtOAc were added to the solution. The organic layer was washed with saturated $NaHCO_3$ and NaCl solutions, dried over $MgSO_4$, and then concentrated under reduced pressure. The Boc group of the residue was removed with TFA (2 mL) at room temperature for 30 min. The solution was then suspended to benzene and lyophilized. N-Acetylation of the residue was carried out with acetic anhydride (24 mg, 0.24 mmol) and TEA (24 mg, 0.24 mmol) in DMF (2 mL). After the solution was allowed to stand at room temperature for 1 h, the reaction mixture was directly purified by preparative HPLC (column, Cosmosil $5C_{18}$, 16.7 × 250 mm; solvent, CH_3CN/0.1% aqueous TFA; gradient, 20–50%, 2% min; flow rate, 9.0 mL/min). The fraction containing pure substance was lyophilized to give **2** as a white powder: yield, 10 mg (31%); FD-MS m/z 541 [$(M + H)^+$]. Amino acid analysis: Lan (0.86), Ile (0.94), Leu (1.00), $MeNH_2$ (1.09).

Boc-Ala-Leu-Cys(Acm)-OMe (3). To a solution of HCl·H-Leu-Cys-(Acm)-OMe[27] (17.0 g, 47.7 mmol) in DMF (60 mL) were added Boc-Ala-OSu (913.7 g, 47.7 mmol) and TEA (12.3 g, 128 mmol) under ice cooling. The mixture was stirred at room temperature overnight and concentrated under reduced pressure. The residue was dissolved in EtOAc and 10% aqueous citric acid. The EtOAc layer was washed with saturated $NaHCO_3$ and NaCl solutions, dried over $MgSO_4$, and then concentrated under reduced pressure. The crystalline residue was recrystallized from EtOAc and hexane: yield, 19.7 g (84.1%); mp 142–144 °C; $[\alpha]^{18}_D$ −85.5° (*c* 1.03, MeOH). Anal. Calcd for $C_{21}H_{38}O_7N_4S$: C, 51.41; H, 7.81; N, 11.42; S, 6.54. Found: C, 51.63; H, 7.85; N, 11.29; S, 6.31.

Boc-Ile-Ala-Leu-Cys(Acm)-OMe (4). The Boc group of **3** (12.0 g, 24.5 mmol) was removed with 4.2 M HCl/MeOH (60 mL) at room temperature for 2 h. An oily residue obtained by concentration under reduced pressure was triturated with ether. To a solution of the residue in DMF (30 mL) were added Boc-Ile-OSu (8.05 g, 24.5 mmol) and TEA (4.96 g, 49.0 mmol) under ice cooling. The mixture was stirred at room temperature overnight and then diluted with H_2O and hexane. The precipitate was filtered and washed with 10% aqueous citric acid, saturated $NaHCO_3$ solution, H_2O, and ether. The crude product was reprecipitated from DMF and H_2O: yield, 13.6 g (91.9%); mp 198–200 °C; $[\alpha]^{15}_D$ −52.2° (*c* 1.08, DMF). Anal. Calcd for $C_{27}H_{49}O_8N_5S$: C, 53.71; H, 8.18; N, 11.60; S, 5.31. Found: C, 53.59; H, 8.15; N, 11.51; S, 5.27.

Boc-D-Cys(Trt)-Ile-Ala-Leu-Cys(Acm)-OMe (5). Peptide **4** (11.0 g, 18.2 mmol) was treated with 4.3 M HCl/MeOH (120 mL) and then coupled with Boc-D-Cys(Trt)-OSu (10.2 g, 18.2 mmol) as described for the preparation of **4** to give a colorless precipitate: yield, 14.7 g (85.0%). A part of the product was recrystallized from $CHCl_3$/MeOH/hexane for elemental analysis: mp 204.5–206 °C; $[\alpha]^{15}_D$ −24.1° (*c* 1.03, DMF). Anal. Calcd for $C_{49}H_{68}O_9N_6S_2$: C, 62.00; H, 7.22; N, 8.85; S, 6.75. Found: C, 61.72; H, 7.31; N, 8.86; S, 6.62.

Boc-D-Cys-Ile-Ala-Leu-Cys-OMe (6). To a solution of **5** (2.07 g, 2.18 mmol) in MeOH (1.0 L) was added I_2 (1.66 g, 6.54 mmol) in MeOH (110 mL) under vigorous stirring.[28] After the solution was stirred for 30 min, a solution of L-ascorbic acid (3.5 g), citric acid monohydrate (6.3 g), and NaOH (2.4 g) in 300 mL of H_2O was added until the color of I_2 disappeared. The precipitate obtained by evaporation of MeOH under reduced pressure was filtered and washed with H_2O and ether. The crude product was purified by silica gel column chromatography (Merck silica gel 60 (230–400 mesh), 70 g, 2.6 × 45 cm, $CHCl_3$:MeOH = 20:1) to give **6**, which was crystallized from $CHCl_3$/MeOH/ether/hexane: yield, 1.01 g, (73.0%); mp 220–222 °C; $[\alpha]^{15}_D$ +26.6° (*c* 1.05, DMF); FD-MS m/z 634 [$(M + M)^+$]. Anal. Calcd for $C_{27}H_{47}O_8N_5S_2$: C, 51.17; H, 7.47; N, 10.05; S, 10.12. Found: C, 50.80; H, 7.48; N, 10.74; S, 10.36.

Boc-D-Ala$_L$-Ile-Ala-Leu-Ala$_L$-OMe (7). To a solution of **6** (103 mg, 0.162 mmol) in anhydrous DMF (50 mL) was added $P(NEt_2)_3$ (250 mg, 1.0 mmol). The mixture was stirred at 25 °C for 2 days and concentrated under reduced pressure. The residue, triturated with hexane, was filtered and washed with hexane. The powder was purified by silica gel column chromatography (Merck silica gel 60 (230–400 mesh), 15 g, 2 × 17 cm, $CHCl_3$:MeOH = 20:1) to give **7**, which was precipitated from MeOH/ether: yield, 40.7 mg (41.7%); mp 211–215 °C; $[\alpha]^{15}_D$ −11.5° (*c* 0.13, DMF); FD-MS m/z 601 [M^+]. Anal. Found: C, 53.04; H, 7.85; N, 11.43; S, 5.27. Calcd for $C_{27}H_{47}O_8N_5S_1 \cdot 0.5H_2O$: C, 53.10; H, 7.92; N, 11.47; S, 5.25. Amino acid analysis: Lan (0.91), Ala (1.00), Ile (0.91), Leu (1.17).

(28) Kamber, B.; Hartmann, A.; Eisler, K.; Riniker, B.; Rink, H.; Sieber, P.; Rittel, W. *Helv. Chim. Acta* **1980**, *63*, 899.

Ac-D-Ala$_L$-Ile-Ala-Leu-Ala$_L$-NHCH$_3$ (8). Peptide **7** (97.5 mg, 0.162 mmol) was dissolved in 6% methylamine/MeOH (3.0 mL). The solution was allowed to stand at room temperature overnight and concentrated under reduced pressure. The Boc group of the residue was removed with TFA (8 mL) as described for the preparation of **2**. N-Acetylation was carried out with succinimido acetate (150 mg, 0.97 mmol) and TEA (98 mg, 0.97 mmol) in DMF (8 mL) at room temperature overnight. Compound **8** thus obtained was purified by preparative HPLC (column, Cosmosil $5C_{18}$, 16.7 × 250 mm; solvent, CH_3CN/0.1% aqueous TFA; gradient, 20–50% (2%/min); flow rate, 8.0 mL/min). The fraction containing the pure substance was lyophilized to give **8** as a powder: yield, 23 mg (26%); FD-MS m/z 542 [M^+]. Amino acid analysis: Lan (1.22), Ala (1.00), Ile (0.92), Leu (1.00), $MeNH_2$ (1.21).

Boc-D-Ala-Leu-Cys(Acm)-OMe (9). Peptide **9** was prepared from HCl·H-Leu-Cys(Acm)-OMe (17.0 g, 47.7 mmol) and Boc-Ala-OSu (13.7 g, 47.7 mmol) as described for the preparation of **3**: yield, 20.3 g, (86.8%); mp 70–72 °C dec; $[\alpha]^{20}_D$ −33.6° (*c* 1.05, DMF). Anal. Calcd for $C_{21}H_{38}O_7N_4S$: C, 51.41; H, 7.81; N, 11.42; S, 6.54. Found: C, 51.40; H, 7.91; N, 11.21; S, 6.15.

Boc-Ile-D-Ala-Leu-Cys(Acm)-OMe (10). Peptide **10** was prepared from peptide **9** (25.6 g, 52.2 mmol) and Boc-Ile-OSu (17.1 g, 52.2 mmol) as described for the preparation of **4**: yield 28.0 g (88.9%); mp 183–185 °C dec; $[\alpha]^{24}_D$ −32.1° (*c* 1.03, DMF). Anal. Calcd for $C_{27}H_{49}O_8N_5S \cdot H_2O$: C, 51.16; H, 8.27; N, 11.26; S, 5.16. Found: C, 52.16; H, 8.26; N, 11.07; S, 4.68.

Boc-D-Cys(Trt)-Ile-D-Ala-Leu-Cys(Acm)-OMe (11). Peptide **11** was prepared from peptide **10** (921.6 g, 35.7 mmol) and Boc-D-Cys(Trt)-OSu (20.0 g, 35.7 mmol) as described for the preparation of **4**. The product was reprecipitated from DMF and H_2O: yield, 29.0 g (85.4%); mp 185–188 °C dec; $[\alpha]^{20}_D$ −12.4° (*c* 1.00, DMF). Anal. Found: C, 61.51; H, 7.20; N, 8.81; S, 6.44. Calcd for $C_{49}H_{68}O_9N_6S_2 \cdot 0.5H_2O$: C, 61.41; H, 7.26; N, 8.77; S, 6.69.

Boc-D-Cys-Ile-D-Ala-Leu-Cys-OMe (12). Peptide **12** (6.00 g, 6.32 mmol) was prepared from peptide **11** as described for the preparation of **6**. Peptide **12** thus obtained was crystallized from MeOH and ether: yield 3.24 g (81.0%); mp 242–244.5 °C dec; $[\alpha]^{20}_D$ +32.6° (*c* 1.01, DMF); FD-MS m/z 634 [$(M + H)^+$]. Anal. Calcd for $C_{27}H_{47}O_8N_5S_2 \cdot 0.5H_2O$: C, 50.45; H, 7.53; N, 10.89; S, 9.98. Found: C, 50.22; H, 7.39; N, 10.85; S, 9.98.

Boc-D-Ala$_L$-Ile-D-Ala-Leu-Ala$_L$-OMe (13). To a solution of **12** (105 mg, 0.166 mmol) in anhydrous THF (250 mL) was added $P(NEt_2)_3$ (250 mg, 1.0 mmol). The mixture was stirred at 25 °C overnight and concentrated under reduced pressure, and the residue was triturated with hexane. A powdery product was filtered and washed with 10% aqueous citric acid, H_2O, and ether. The raw product was purified by silica gel column chromatography (Merck silica gel 60 (230–400 mesh), 4 g, 1.4 × 9 cm, $CHCl_3$:MeO = 20:1) to give **13**, which was precipitated from MeOH/ether: yield, 66.3 mg (66.5%); mp 120–121 °C; $[\alpha]^{20}_D$ −11.3° (*c* 1.03, DMF); FD-MS m/z 602 [$(M + H)^+$]. Anal. Calcd for $C_{27}H_{247}O_8N_5S_2 \cdot 0.5H_2O$: C, 50.45; H, 7.53; N, 10.89; S, 9.98. Found: C, 50.22; H, 7.39; N, 10.85; S, 9.98. Amino acid analysis: Lan (1.03), Ala (1.00), Ile (0.88), Leu (0.98).

Ac-D-Ala$_L$-Ile-D-Ala-Leu-Ala$_L$-NHCH$_3$ (14). Peptide **14** was prepared from peptide **13** (46.6 mg, 77.4 μmol) was described for the preparation of **8**: yield, 15 mg (36%); FD-MS m/z 542 [M^+]. Amino acid analysis: Lan (1.11), Ala (1.00), Ile (0.94), Leu (1.00), $MeNH_2$ (1.13).

Ac-Dha-NHCH$_3$ (15). Peptide **15** was prepared by the dehydration of Ac-Ser-$NHCH_3$ (480 mg, 3 mmol) in a solution of cupric chloride (150 mg, 1.5 mmol) and EDC (690 mg, 1.2 mmol) in 5 mL of DMF. After 6 h, the reaction mixture was dried under reduced pressure and purified by silica gel column chromatography eluted with 1:2 $CHCl_3$/AcOEt. The residue was triturated with Et_2O and recrystallized from AcOEt to give colorless prisms: yield, 350 mg (82%); ^1H NMR (DMSO-d_6) δ 9.05 (s, Dha HN), 8.26 (q, $NHCH_3$ HN), 6.01 (s, Dha Hβ), 5.33 (s, Dha Hβ), 2.68 (d, $NHCH_3$ H_3C), 2.02 (s, Ac H_3C); FAB-MS m/z 143 [$(M + H)^+$]. Anal. Calcd for $C_6H_{10}O_2N_2$: C, 50.70; H, 7.04; N, 19.72. Found: C, 50.93; H, 7.30; N, 20.15.

X-ray Structure Determination. Crystals of Ac-Dha-NHMe were examined. Determination of cell constants, crystal system and symmetry, and data collection were carried out on a Siemens R3m/V four-circle diffractometer with Mo Kα radiation by using a highly oriented graphite crystal in the range 4–110° of 2θ. A 2θ–θ scan type with variable speed (2.0–5.0 deg min^{-1}) and a scan range of 0.5° + Kα separation were selected. Background counts were taken at the beginning and at the end of the scan. Three standard reflections were monitored every 60 reflections to detect crystal decay; no significant changes in their intensities were observed. The *h*,*k*,*l* ranges were 0 to 8, 0 to 11, and −17 to 17,

respectively. A total of 2235 reflections were measured, 1710 of which had $F > 4.0\sigma$ and thus were considered "observed".

The structure was determined by direct methods with the SHELXTL PLUS program on a Micro-VAX II computer. Full-matrix least-squares refinement minimizing the quantities $\sum w(F_o - F_c)$ and $1/w = \sigma^2(F) + 0.0010F^2$ was used. All non-hydrogen atoms were refined anisotropically, while hydrogen atoms were refined isotropically. The total number of parameters refined was 242.

NMR Spectroscopy. The NMR spectra were recorded on a GN-500 spectrometer. Samples were dissolved and lyophilized in DMSO-d_6 purchased from Merck Sharp and Dohme Canada Ltd. The dry sample was redissolved in DMSO-d_6 at concentrations between 2 and 5 mM, degassed by the freeze–pump–thaw method, and flame sealed. DMSO-d_6 (δ = 2.49 ppm) was used as an internal standard. Temperatures were maintained at given values within ±0.1 °C during measurements.

One-dimensional spectra were accumulated with 32 transients of 16K data points with spectral widths of approximately ±3000 Hz and relaxation delays of 3 s between successive scans. The temperature coefficients for the amide resonances were measured from spectra obtained at 5 °C intervals over the range 25–60 °C. Proton–proton coupling constants were measured from the spectrum at 35 °C.

The homonuclear Hartmann–Hahn (HOHAHA) experiments were performed using the MLEV-17 sequence and time proportional phase incrementation.[29] A mixing time of 75 ms with a spin-locking field of 10.2 kHz was employed. The rotating frame nuclear Overhauser (ROESY) experiments were carried out with mixing times of 150, 300, and 450 ms.[30] A spin-locking field of 2.5 kHz was used, and the carrier frequency was varied per experimental run to minimize and identify experimental artifacts.[31] The COSY, HOHAHA, and ROESY experiments were obtained using 32 scans per t_1, with 2K data points in the t_2 domain and 256 points in the t_1 domain. Zero-filling was applied once in the t_1 and t_2 domains, resulting in a final data matrix of 4K × 512 points. Multiplication with either a sine or Gaussian function (LB = 1/AT in t_2; LB = 4/AT in t_1) was employed. All 2-D spectra were obtained at 35 °C.

Semiempirical Quantum Mechanical Calculations. MOPAC[32] version 4.0 was used with the AM1 parameter set[33] and a gradient norm of 0.1. Conformational energy maps of the ϕ–ψ torsion space were determined for each compound in vacuo by fixing ϕ and ψ at points on a 30-deg grid and optimizing all other internal coordinates. The global energy minima for each compound were determined by full geometry optimization within each local minimum of the ϕ–ψ map.

Hydrogen atom positions in the asymmetric unit of Ac-Dha-NHMe were optimized with the coordinates of heavy atoms fixed at their crystallographic positions. All bond lengths, bond angles, and out-of-plane angles used as reference values in subsequent simulated annealing were determined from the resulting structure. The torsion angles used as reference values were derived from the calculated global energy minima in vacuo.

Force Field Parametrization. In the determination of CVFF parameters for dehydroalanine, the C_α and C_β carbons were assigned the atom type "c=", the default atom type for a double-bonded carbon. All other atom types were the same as assigned by the CVFF to conventional residues.[25] Partial changes assigned to atoms in the dehydroalanine residue were derived from those calculated by MOPAC for the global minimum energy conformations. The Lennard-Jones parameters for c= were taken from the CVFF. For simulating dehydroalanine, 102 additional parameters were necessary which were not required for the standard amino acid residues. Of these parameters, all of which involved the c= atom type, only 41 existed in the CVFF.[34] These 102 parameters were optimized by Monte Carlo simulated annealing.[35] What follows is a brief outline of the annealing process and then the experimental particulars.

Each step of simulated annealing began with a small random modification to a force field parameter. This was followed by conformational energy minimization of Ac-Dha-NHMe using the new parameter set. The internal coordinates of the resulting conformation were quantitatively compared to reference values by evaluating a target function, F. The modified parameter set served as the starting point for subsequent modification unless $\exp[-\Delta F/T]$ was less than a random number between 0 and 1, in which case the previous parameter set was restored. T in this equation is an abstract temperature, which was gradually decreased to improve convergence. This cycle was repeated 7500–15000 times for each of five runs.

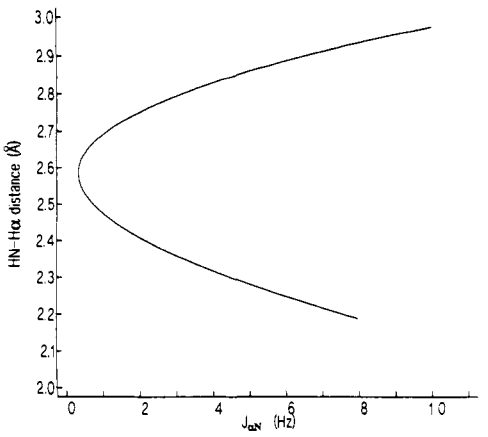

Figure 1. Relationship of the $J_{\alpha N}$ coupling constant to the HN–Hα distance, as predicted using standard geometries from the DISCOVER residue library and the Karplus-type equation described in the text.

For each cycle, one of the 102 parameters involving c= was randomly selected and randomly altered by a small increment. The new value for the parameter was required to be between specified lower and upper bounds. The intent of these bounds was to allow a reasonable range of variation and yet maintain some consistency with the CVFF. This specified range for equilibria was ±0.1 Å and ±15° about the reference bond lengths and angles, respectively. The allowable range for force constants and order parameters was 50–150% of the corresponding values given in the CVFF for existing c= atom parameters. When no such parameters existed, 50–150% of the corresponding parameters involving either the c or c′ atom types was used. The starting parameter set differed from the default CVFF parameter set in that values for the 61 missing parameters were inferred from other parameters and in that a 2-fold, rather than a 3-fold, symmetric potential was assumed for the dehydroalanine ϕ torsion.

The conformational energy of Ac-Dha-NHMe in vacuo was then minimized by DISCOVER using these new parameters with 2000 steps of the va09a minimization algorithm and a convergence threshold of 0.001 kcal/Å. The starting conformation had ϕ and ψ torsions adjusted to 190° and 170°, respectively, to bias the resulting conformation toward one of two symmetry-related minima. The minimization was followed by evaluation of a target function of the form $F = \sum(\text{ic} - \text{ic}_{\text{ref}})^2/w_{\text{ic}}^2 + w_{\text{conf}}(\Delta E_{\text{conf}} - \Delta E_{\text{ref}})$. The "ic" refer to values of various internal coordinates (viz., bond lengths, bond angles, torsions, and out-of-plane angles). The reference values, ic_{ref}, for these internals were derived from crystallographic coordinates and MOPAC calculations as described above. The w_{ic} weights are defined as the difference between the values for a given internal measured for the two molecules in the unit cell plus the experimental uncertainties in each value. This was intended to normalize the contributions measured in different units and dimensionality. The ΔE_{conf} term represents the energy difference between the calculated minimum energy conformation and the conformation with ϕ and ψ torsions of 0°. The ΔE_{ref} value represents the difference between the global maximum and minimum energies as determined from the MOPAC ϕ–ψ map. The w_{conf} used was 0.5. This term was necessary since an "inverted" version of the ϕ–ψ map emerged during a preliminary run.

The temperature, T, was adjusted every 50 cycles according to the formula $T_{i+50} = T_i C_{\text{col}}$, where C_{col} is the greater of 0.95 or $1 - (20C_p)^{-1}$, and $C_p = (\langle F^2\rangle - \langle F\rangle^2)/T_i^2$. C_p, analogous to the heat capacity, was calculated over the previous 50 cycles. For the five runs, the initial temperatures were 100.0 for two runs, 10.0 for two runs, and 1.0 for one run.

Conformational Analysis. Distance constraints were derived from the observed NOEs and $J_{\alpha N}$ coupling constants, which were used in DGEOM[36] distance geometry calculations. The resulting structures were then subjected to unconstrained conformational energy minimizations using DISCOVER with our optimized force field parameters. The resulting struc-

(29) Davis, D.; Bax, A. *J. Am. Chem. Soc.* **1985**, *107*, 2820–2821.
(30) Bothner-By, A. A.; Stephens, R. L.; Lee, J.; Warren, C. D.; Jeanloz, R. W. *J. Am. Chem. Soc.* **1984**, *106*, 811–813.
(31) Bax, A.; Davis, D. G. *J. Magn. Reson.* **1985**, *63*, 207–213.
(32) MOPAC version 4.0: Stewart, J. J. P. *QCPE* No. 455, 1987.
(33) Dewar, M. J. S.; Zoebisch, E. G.; Healy, E. F.; Stewart, J. J. P. *J. Am. Chem. Soc.* **1985**, *107*, 3902–3909.
(34) The complete listing of our changes to Biosym's consistent valence force field parameters and residue library is available with the supplementary material.
(35) Metropolis, M.; Rosenbluth, A.; Rosenbluth, M.; Teller, A.; Teller, E. *J. Chem. Phys.* **1953**, *21*, 1987–1091.
(36) DGEOM: Blaney, J. M.; Crippen, G. M.; Dearing, A.; Dixon, J. S. *QCPE* No. 590, 1989.

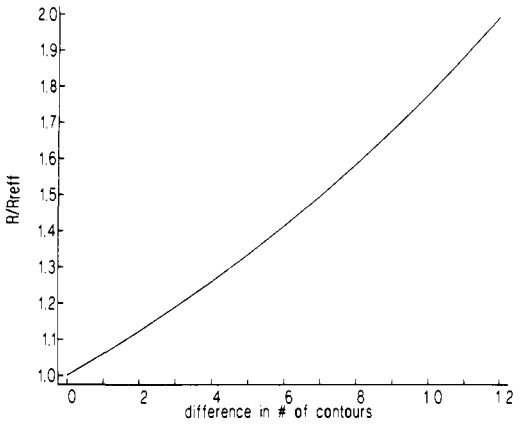

Figure 2. Relationship of the relative interproton distances (R/R_{reff}) to relative ROESY cross-peak height as determined by contour counts. In this model, cross-peaks are assumed to be a Gaussian of rotation and their volumes to be linearly proportional to R^{-6}.

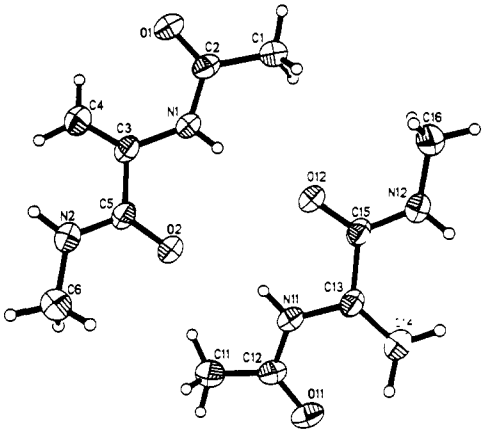

Figure 3. Crystallographic structure of the two molecules in the asymmetric unit of *N*-acetyldehydroalanine *N'*-methylamide. The atoms are drawn with 30% probability ellipsoids.

tures were filtered for compatibility with backbone NOEs, $J_{\alpha N}$ coupling constants, and temperature coefficients. The determination of these constraints and the assessment of compatibility with NMR data are described below.

Backbone torsions were calculated using the following Karplus-type equation: $J_{\alpha N} = A\cos^2|\phi \pm 60°| - B\cos|\phi \pm 60°| + C$[+ for a D and − for an L residue, respectively], where $(A,B,C) = (9.4,1.1,0.4)$ Hz and the $J_{\alpha N}$ coupling constants were multiplied by a correction factor of 1.09.[37] For $J_{\alpha N} \geq 8.0$ Hz, the above relation yields two values for ϕ. However, these two torsions correspond to a single HN−Hα distance (Figure 1). Even for $J_{\alpha N} \leq 8.0$ Hz, only two distances are determined, and these differ substantially for $J_{\alpha N} \geq 3$ Hz. Thus, for residues with $J_{\alpha N} \geq 8.0$ Hz, we constrained the intraresidue HN−Hα distance to the $J_{\alpha N}$-determined distance ±0.05 Å in our distance geometry calculations.

The NOEs were quantified by contour counting. Normalization across different experiments was achieved by comparing diagonal peak intensities. To convert contour counts into volumes, each cross-peak was assumed to be a Gaussian of rotation, for which volume is a linear function of height. Each contour represents a factor of $(2)^{1/2}$ in relative height and relative volume. With the standard assumption that cross-peak volume varies as R^{-6}, a formal relationship of countour count to relative interproton distance, R/R_{reff}, can be determined (Figure 2). Intraresidue HN−Hα distances were used as internal references in calibrating this curve. Appropriate experimental cautions were taken to minimize and identify frequency offset effects on NOE intensity,[31] as described above. This model neglects the effects of nonuniform correlation times and spin diffusion. On the basis of published work on molecules of similar size and constraint, differences in correlation time probably account for an error of less than 10%.[38,39] Spin diffusion is generally considered neglgible in the rotating frame.[39] To accommodate the error in these assumptions, the contour count was used only to determine very coarse-grained interresidue distance constraints on the backbone hydrogen atoms; van der Waals radii: 2.5, 2.5–3.0, or 3.0–4.0 Å. A repulsive minimum distance constraint of 3.5 Å was used between backbone hydrogens where the NOE was clearly absent. For interresidue NOEs involving side chains, the respective hydrogens were constrained to within 4.0 Å of each other. For NOEs involving methyl hydrogens, the constrains were drawn to the methyl carbon, and 1.0 Å was added to the range limit.[40] The distance geometry program DGEOM[36] was used to generate structures compatible with NOEs.

The comparison of calculated structures with NOE data follows a scheme which assigns an index of agreement with each NOE.[41] Strong NOEs result in an index of 30 points if the appropriate hydrogens are within 2.5 Å of each other, and this index decreases linearly to zero over the range 2.5–3.0 Å. Larger separations result in negative indices. For medium NOEs, an index of 20 is awarded for separations up to 3.0 Å, decreasing linearly to zero over the range 3.0–4.0 Å. For weak NOEs, an index of 10 is awarded for separations up to 4.0 Å, decreasing linearly to zero over the range 4.0–6.0 Å. Ambiguous NOEs, such as those involving methylene or methyl protons, are evaluated on the basis of the smallest separation of candidate protons.

The ϕ torsions from these NOE-compatible structures were compared to the torsions computed from the $J_{\alpha N}$ coupling constants. Allowed torsion ranges were calculated for each $J_{\alpha N} \pm 0.3$ Hz to reflect the experimental resolution. Conformations with high indices of agreement with NOEs and which were within 15° of the allowed torsion ranges were selected. These structures were then examined for compatibility with the temperature coefficients—defined as the proximity of carbonyl oxygens to amide protons with temperature coefficients greater than −2.5 ppb/K. Lastly, the remaining structures were examined for compatibility with stereospecific NOEs involving the lanthionine methylene protons. For each molecule, a cluster of conformations with similar backbones was determined. Using these common backbone conformations, the accessible side chain conformations for the Ile and Leu residues were determined by systematically rotating about the χ_1 torsions of these residues and minimizing conformational energy.

Crystal Simulation. The dynamics of the two molecules in the crystallographic asymmetric unit was simulated in the crystalline environment using our derived parameters. Periodic boundary conditions were employed with a 20-Å cutoff and 1.5-Å switching distance. The coordinates, space group, and lattice vectors from the X-ray diffraction data were used to generate all of the appropriate "ghost" molecules within this cut-off range. The hydrogen atom positions were first allowed to adjust by 500 steps of steepest descent energy minimization, with the heavy atoms tethered to their initial positions by a force of 2000 kcal/Å. This was followed by 500 steps of unconstrained steepest descent minimization. Dynamics then proceeded from this relaxed conformation for 50 ps coupled to a constant temperature bath of 300 K and pressure bath of 1 bar and a step size of 1 fs.

All of the MOPAC calculations were run on the SDSC Cray Y-MP computer. The simulated annealing and cyclic fragment minimizations employed DISCOVER Ver. 2.5 on the SDSC Cray Y-MP. The crystal simulation was carried out using DISCOVER Ver. 2.7 on the Silicon Graphics IRIS 340 computer in the UCSD Department of Chemistry computer facility. All other calculations utilized our own Silicon Graphics Personal IRIS.

Results and Discussion

Synthesis. The fragment derivatives were characterized by NMR and mass spectrometry, amino acid analysis, and microchemical analysis. The desired products were synthesized in good yields and with high purity.

X-ray Structure Determination. *N*-Acetyldehydroalanine *N'*-methylamide crystallized in the monoclinic $P2_1/c$ space group with two independent molecules in the asymmetric unit[42] (see Figures 3 and 4). The final R index and goodness of fit were 0.063 and 2.31, respectively, with largest and mean Δ/σ values of 0.258 and −0.001. Crystallographic internal coordinates for both molecules in the asymmetric unit (designated 1 and 2) are listed in Tables

(37) Bystrov, V. F.; Ivanov, V. T.; Portnova, S. L.; Balashova, T. A.; Ovchinnikov, Y. A. *Tetrahedron* **1973**, *29*, 873–877.
(38) Davis, D. G. *J. Am. Chem. Soc.* **1987**, *109*, 3471–3472.
(39) Kazmierski, W. M.; Yamamura, H. I.; Hruby, V. J. *J. Am. Chem. Soc.* **1991**, *113*, 2275–2283.
(40) Wüthrich, K.; Billeter, M.; Bruan, W. *J. Mol. Biol.* **1983**, *169*, 949–961.
(41) Feinstein, R. D.; Polinsky, A.; Douglas, A. J.; Beijer, C. M. G. F.; Chadha, R. K.; Benedetti, E.; Goodman, M. *J. Am. Chem. Soc.* **1991**, *113*, 3467–3473.

(42) The complete listing of our crystallographic parameters and results is available with the supplementary material.

Table I. Observed and Calculated Bond Lengths

bond		X-ray diffraction		crystal simulation		energy minimization	
		1	2	1	2	MOPAC	DISCOVER
Ac CA	Ac HA	0.938 (0.028)	0.916 (0.024)	1.111 (0.043)	1.107 (0.032)	1.117	1.105
		1.119	1.119				
Ac CA	Ac C	1.480 (0.005)	1.483 (0.004)	1.519 (0.030)	1.512 (0.037)	1.511	1.508
Ac C	Ac O	1.225 (0.004)	1.223 (0.003)	1.230 (0.022)	1.232 (0.027)	1.245	1.230
Ac C	Dha N	1.342 (0.004)	1.354 (0.004)	1.337 (0.026)	1.343 (0.032)	1.389	1.340
Dha N	Dha HN	0.843 (0.034)	0.833 (0.032)	1.025 (0.009)	1.024 (0.009)	0.998	1.017
		1.007	1.006				
Dha N	Dha CA	1.400 (0.004)	1.402 (0.004)	1.427 (0.033)	1.419 (0.045)	1.401	1.405
Dha CA	Dha CB	1.323 (0.005)	1.326 (0.004)	1.326 (0.028)	1.328 (0.028)	1.347	1.325
Dha CB	Dha HB1	0.990 (0.032)	0.956 (0.032)	1.099 (0.031)	1.103 (0.040)	1.099	1.101
		1.103	1.102				
Dha CB	Dha HB2	0.929 (0.034)	0.932 (0.033)	1.101 (0.035)	1.103 (0.039)	1.097	1.098
		1.097	1.097				
Dha CA	Dha C	1.502 (0.004)	1.490 (0.004)	1.525 (0.032)	1.497 (0.031)	1.518	1.489
Dha C	Dha O	1.231 (0.003)	1.228 (0.003)	1.236 (0.020)	1.235 (0.020)	1.249	1.233
Dha C	NMe N	1.328 (0.004)	1.324 (0.004)	1.330 (0.028)	1.330 (0.031)	1.375	1.328
NMe N	NMe HN	0.839 (0.032)	0.866 (0.033)	1.033 (0.020)	1.033 (0.018)	0.992	1.026
		0.993	0.995				
NMe N	NMe CA	1.440 (0.004)	1.433 (0.005)	1.475 (0.028)	1.478 (0.032)	1.428	1.470
NMe CA	NMe HA	0.931 (0.035)	0.935 (0.034)	1.110 (0.038)	1.113 (0.040)	1.124	1.107
		1.123	1.123				

Table II. Observed and Calculated Bond Angles

bond angle			X-ray diffraction		crystal simulation		energy minimization	
			1	2	1	2	MOPAC	DISCOVER
Ac HA	Ac CA	Ac C	108.9 (1.8)	113.4 (2.0)	111.4 (4.6)	111.3 (4.8)	109.9	111.4
			110.2	110.4				
Ac CA	Ac C	Ac O	120.9 (0.3)	122.1 (0.3)	117.9 (3.1)	118.7 (3.0)	121.4	119.8
Ac CA	Ac C	Dha N	116.7 (0.3)	115.9 (0.2)	116.1 (2.7)	115.5 (3.0)	116.1	115.4
Ac O	Ac C	Dha N	122.3 (0.3)	122.0 (0.3)	125.7 (2.4)	125.3 (2.6)	122.5	124.8
Ac C	Dha N	Dha CA	127.5 (0.2)	127.1 (0.2)	128.4 (1.9)	128.1 (2.1)	126.1	127.9
Ac C	Dha N	Dha HN	116.6 (2.2)	113.1 (2.3)	116.8 (5.3)	116.0 (5.3)	118.1	117.7
			117.9	118.1				
Dha HN	Dha N	Dha CA	115.8 (2.2)	119.3 (2.3)	112.3 (5.6)	113.6 (5.2)	115.3	114.4
			114.6	114.8				
Dha N	Dha CA	Dha CB	124.7 (0.3)	126.1 (0.3)	126.6 (2.1)	128.5 (2.6)	126.4	127.8
Dha CA	Dha CB	Dha HB1	118.9 (1.8)	123.2 (1.8)	123.8 (4.6)	123.6 (4.7)	123.0	122.6
			122.6	123.0				
Dha CA	Dha CB	Dha HB2	120.3 (2.0)	120.2 (1.9)	124.2 (4.7)	124.0 (4.5)	121.6	124.1
			124.2	123.0				
Dha HB1	Dha CB	Dha HB2	120.7 (2.7)	116.5 (2.6)	111.9 (5.0)	112.3 (5.0)	115.4	113.3
			113.2	114.0				
Dha N	Dha CA	Dha C	111.4 (0.2)	111.6 (0.2)	111.2 (2.2)	110.8 (2.5)	113.2	111.3
Dha CB	Dha CA	Dha C	123.8 (0.3)	122.1 (0.3)	122.0 (2.3)	120.4 (3.0)	120.4	120.9
Dha CA	Dha C	Dha O	119.7 (0.2)	120.1 (0.2)	120.1 (3.4)	119.7 (3.4)	121.0	120.0
Dha CA	Dha C	NMe N	117.8 (0.2)	117.5 (0.2)	119.9 (2.2)	118.5 (2.4)	116.9	117.6
Dha O	Dha C	NMe N	122.5 (0.2)	122.4 (0.3)	119.7 (2.1)	121.6 (2.7)	122.1	122.4
Dha C	NMe N	NMe CA	122.0 (0.3)	123.4 (0.3)	123.1 (2.0)	122.8 (2.4)	122.9	122.4
Dha C	NMe N	NMe HN	118.3 (2.3)	120.5 (2.1)	113.3 (4.0)	112.0 (3.9)	119.1	112.8
			121.4	120.2				
NMe HN	NMe N	NMe CA	119.7 (2.3)	116.1 (2.0)	122.0 (3.6)	123.2 (3.9)	117.9	124.8
			116.6	116.1				
NMe N	NMe CA	NMe HA	111.7 (2.1)	111.6 (2.0)	111.6 (4.3)	111.6 (4.0)	110.1	111.6
			109.9	110.0				

Table III. Observed and Calculated Torsion Angles

torsion angle				X-ray diffraction		crystal simulation		energy minimization	
				1	2	1	2	MOPAC	DISCOVER
Ac CA	Ac C	Dha N	Dha CA	186.5	179.2	178.4 (6.2)	187.5 (6.1)	176.2	178.4
Ac C	Dha N	Dha CA	Dha C	162.6	187.7	167.0 (7.6)	181.7 (7.5)	172.8	152.6
Ac C	Dha N	Dha CA	Dha CB	340.9	12.7	345.0 (9.0)	4.9 (9.3)	351.1	329.3
Dha N	Dha CA	Dha CB	Dha HB1	357.3	354.5	0.5 (5.6)	357.8 (6.4)	359.9	1.8
				1.2	357.5				
Dha N	Dha CA	Dha CB	Dha HB2	179.8	178.1	180.6 (5.5)	177.5 (6.4)	180.5	182.1
				181.0	177.2				
Dha N	Dha CA	Dha C	NMe N	190.6	154.1	201.4 (5.9)	131.3 (6.7)	221.1	233.1
Dha CA	Dha C	NMe N	NMe CA	181.0	179.6	184.3 (5.3)	178.5 (4.7)	182.3	181.0

I–IV. The internal coordinates after MOPAC refinement of the hydrogen positions are shown below the experimental coordinates. The standard deviations of each coordinate over the course of the simulation are shown parenthetically, as are the experimental uncertainties for the bond lengths and angles.

Both molecules in the asymmetric unit are roughly planar. The ϕ torsions are both within 20° of trans orientation, while the ψ torsions are both within 30° of trans orientation.

Table IV. Observed and Calculated Out-of-Plane Angles

out-of-plane angle				X-ray diffraction		crystal simulation		energy minimization	
				1	2	1	2	MOPAC	DISCOVER
Ac CA	Ac C	Dha N	Ac O	184.0	179.9	179.5 (6.4)	180.0 (8.6)	180.9	180.8
Dha HN	Dha N	Ac C	Dha CA	176.0	188.6	183.0 (19.5)	169.8 (15.6)	188.4	179.4
				177.0	179.3				
Dha C	Dha CA	Dha CB	Dha N	178.2	185.5	177.8 (5.2)	183.5 (6.4)	178.2	176.5
Dha HB1	Dha CB	Dha HB2	Dha CA	182.5	183.3	180.2 (4.1)	179.7 (5.0)	180.6	180.2
				179.7	179.7				
Dha CA	Dha C	NMe N	Dha O	180.4	179.2	182.1 (5.2)	178.0 (6.4)	178.9	180.9
NMe HN	NMe N	NMe CA	Dha C	179.6	181.8	183.7 (12.8)	173.8 (13.6)	182.8	179.7
				180.0	185.3				

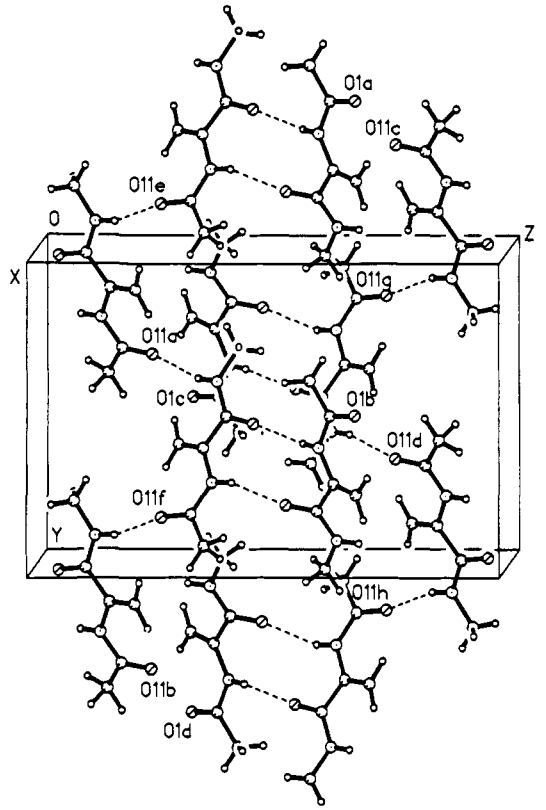

Figure 4. Unit cell packing diagram of *N*-acetyldehydroalanine *N'*-methylamide. Hydrogen atoms are omitted for clarity.

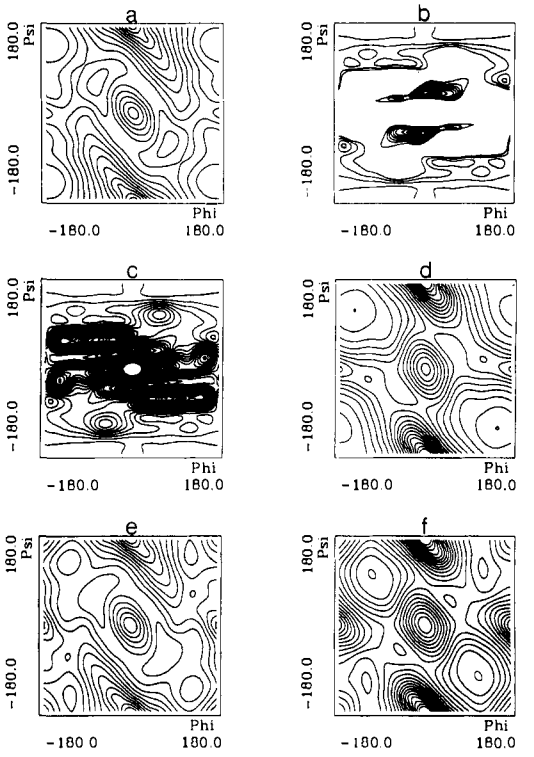

Figure 5. ϕ–ψ conformational energy maps. Figure 5a–d represent maps calculated for *N*-acetyldehydroalanine *N'*-methylamide using (a) the MOPAC AM1 force field; (b) the DISCOVER CVFF force field and default parameter assignments; (c) our starting parameter set; and (d) our final parameter set. Figure 5e,f represent maps for *N*-acetyl-α-amino-α,β-dehydrobutyric acid *N'*-methylamide using (e) the MOPAC AM1 force field and (f) our final parameter set. Each contour represents a difference of 1 kcal/mol.

Simulated Annealing. The quality of the determined force field parameters is reflected in the comparison of the internal coordinates of the two molecules of the asymmetric unit from X-ray diffraction and from our crystal simulation (Tables I–IV). The rms deviations between the simulation and experimental data for heavy atom bond lengths, bond angles, and torsions were 0.021 Å, 1.9°, and 8.7°, respectively. Only the final 40 ps of the simulation were used in determining these time-averaged coordinates, by which time the temperature, pressure, and total energy had reached an apparent equilibrium. The largest differences in the bond lengths and angles occurred in the terminal acetyl and *N*-methylamide groups.

Another indication of the validity of our parameters is the close agreement of the MOPAC- and DISCOVER-generated ϕ–ψ maps (Figure 5a,d, respectively). The ϕ–ψ maps determined using the DISCOVER default parameters or the "best guess" starting parameter set (Figure 5b,c, respectively) show little similarity to the MOPAC results. The final parameter set reproduced the distribution of minima and maxima, as well as the overall twist of the potential energy surface. No spurious energy minima were observed along the $\psi = 0$ axis, as had been reported earlier.[24]

The changes in the parameters during the course of annealing suggest increased double bond character for the N–C_α bond in dehydroalanine. The force constant for N–C_α bond stretching increased, while the equilibrium bond length diminished. The ϕ torsional potential barrier also increased. Recently, another group parametrized the AMBER force field for modeling α,β-unsaturated amino acids. Their parameters were derived using experimental measurements from the literature, ad hoc quantum mechanical calculations, and inference from existing parameters.[43] They suggest ϕ and ψ torsional potentials which are 3–4-fold higher than what we have determined. However, the absence of cross terms in the AMBER force field make direct comparisons difficult.

As a test of the generality of our parameters to other α,β-unsaturated amino acids, MOPAC and DISCOVER ϕ–ψ maps were generated for *N*-acetyl-α-amino-α,β-dehydrobutyric acid *N'*-methylamide (Figure 5e,f, respectively). The additional parameters necessary for the DISCOVER simulation of the α-amino-α,β-dehydrobutyric acid residue (DHb) were present in the CVFF. Again, the similarity of the distribution of minima and maxima is apparent. Of particular interest is the splitting of the global minima, which are in the upper left and lower right quadrants of the Ac-Dha-NHMe ϕ–ψ map. The global minima for Ac-Dhb-NHMe are in the upper left and lower right quadrants, while local minima are in the upper right and lower left corners. This is evident for both maps. Again the same overall twist of the ϕ–ψ

(43) Alagona, G.; Ghio, C.; Pratesi, C. *J. Comput. Chem.* **1991**, *12*, 934–942.

Table V. Observed $J_{\alpha N}$ and Calculated Torsion Angles[a]

residue	Dha[4] $J_{\alpha N}$	Dha[4] $\phi_{Bystrov}$	Dha[4] ϕ_{calcd}	Dha[4] ψ_{calcd}	D-Ala[4] $J_{\alpha N}$	D-Ala[4] $\phi_{Bystrov}$	D-Ala[4] ϕ_{calcd}	D-Ala[4] ψ_{calcd}	L-Ala[4] $J_{\alpha N}$	L-Ala[4] $\phi_{Bystrov}$	L-Ala[4] ϕ_{calcd}	L-Ala[4] ψ_{calcd}
D-Ala$_L$[2]	8.1	93	77	23	8.8	141	140	56	8.5	144	141	45
Ile[3]	8.3	−94	−89	68	9.3	−104	−103	84	9.0	−139	−152	−77
X[4]			124	−144	7.5	74	80	−95	7.7	−90	−91	91
Leu[5]	7.7	−90	−101	84	8.0	−92	−95	121	7.6	72	70	158
Ala$_L$[6]	8.2	−93	−97	86	9.0	−101	−87	84	8.9	−140	−128	143

[a] The $J_{\alpha N}$ values are measured in hertz. The torsions are measured in degrees. Although as many as four $\phi_{Bystrov}$ torsion values can be calculated from a given $J_{\alpha N}$, as described in the text, we have listed the single value which most closely approximates the ϕ_{calcd}.

Table VI. Observed Temperature Coefficients of the Amide Protons

residue	Dha[4] $\Delta\delta/\Delta T$, −ppb/K	D-Ala[4] $\Delta\delta/\Delta T$, −ppb/K	L-Ala[4] $\Delta\delta/\Delta T$, −ppb/K
D-Ala$_L$[2]	3.1	3.5	3.8
Ile[3]	4.2	2.9	1.9
X[4]	1.3	5.8	3.3
Leu[5]	3.4	2.8	−0.5
Ala$_L$[6]	2.6	3.6	7.6
NHMe[7]	4.3	5.7	6.1

map is present. The global minima of the of the MOPAC ϕ–ψ map are at $\phi = \pm 80$, $\psi = \mp 55$, with adjacent local minima at $\phi = \pm 130$, $\psi \mp 134$. These merge in the DISCOVER ϕ–ψ map to yield global minima at $\phi = \pm 112$, $\psi = \mp 109$. In either case, the α-amino-α,β-dehydrobutyric acid residue adopts a less planar conformation than dehydroalanine. Dehydrophenylalanine is also less planar.[24]

This is, to our knowledge, the first use of simulated annealing in force field parametrization. The method has been easy to implement despite the high dimensionality of this optimization problem. Furthermore, the flexibility of the approach allows one to readily include additional constraints based on experimental or computational data. We restricted ourselves to constraints derived from X-ray crystallography and semiempirical calculations, which for most small organic compounds are readily determined or obtained from the literature. However one could easily include force constants from vapor-phase IR spectroscopy and/or ab initio calculations as additional terms in the target function or as bounds in the parameter incrementation. Even local minima or maxima in a calculated ϕ–ψ map could serve as constraints, such as our ΔE_{ref} term. Besides providing direct constraints on force constants, the inclusion of such data would improve the data-to-parameter ratio. Overall, we employed 112 internal coordinate measurements and 91 independent MOPAC conformational energy calculations in the determination and subsequent validation of 102 parameters for a data-to-parameter ratio of 2.

The subsequent calculations were carried out using the parameter set which yielded the lowest target function value. The other four runs were trapped in distinct local minima of the parameter space (see Figure 6). We are currently investigating more sophisticated cooling and incrementation schedules, which will surmount this multiple minimum problem and ensure convergence to globally optimized parameters independent of initial conditions.

Application to Structural Determination by NMR Spectroscopy. Significant conformational effects of dehydroalanine were evident in our comparison of cyclic peptides. Although the $J_{\alpha N}$ values (Table V) observed for the three molecules were similar, considerable differences existed in temperature coefficients (Table VI) and NOEs (Tables VII–IX) across the lanthionine bridge. Our calculated structures demonstrate that the L-Ala[4] analog assumes an inverse γ-turn about the central alanine residue while the D-Ala[4] analog assumes a γ-turn at the same position (Figure 7). Both molecules demonstrate evidence for a pair of reciprocal Ile–Leu hydrogen bonds, although these are more apparent in the temperature coefficients and calculated geometry for the L-Ala[4] compound. In contrast, the Dha[4]-containing peptide assumes an inverse γ-turn about the neighboring Ile[3] residue, which makes the overall conformation more planar. Similar effects on the preceding residue have been observed in linear dehydroalanine-containing peptides.[22] The ϕ and ψ torsions calculated for the dehydroalanine were 124° and −144°, respectively. The conformation is slightly less planar than the average conformation

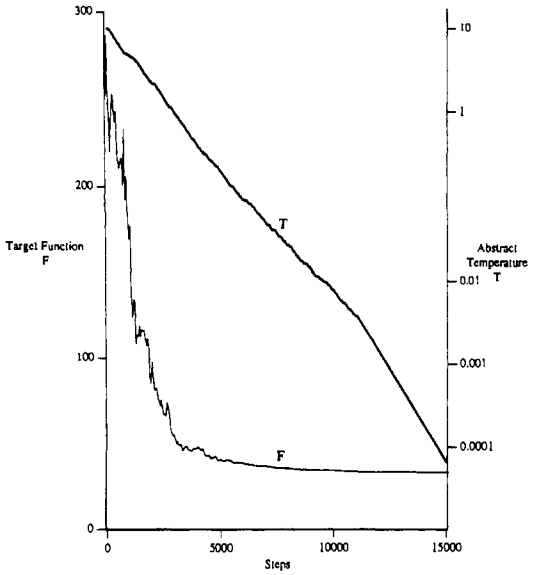

Figure 6. Variation of target function (F) and temperature (T) with the annealing step from the run which resulted in the lowest target function value. The target function measures the difference between the internal coordinates of *N*-acetyldehydroalanine *N'*-methylamide as determined by crystallography and MOPAC semiempirical quantum mechanical calculations and those determined by DISCOVER conformational energy minimization in vacuo. The DISCOVER force field parameters specific to the dehydroalanine residue were altered randomly and the temperature was gradually reduced during the course of annealing, as described in the text.

Table VII. Nisin Ring A Nuclear Overhauser Effects[a]

		Ac	D-Ala$_L$				Ile			DhA			Leu		Ala$_L$				NMe	
		Me	N	α	βd	βu	N	α	β	N	βd	βu	N	α	N	α	βd	βu	N	Me
Ac	Me		M																	
D-Ala$_L$	N			M	W	W	M													
	α				S	–	W											–		
	βd					–												–		
	βu						W			W						–	–	–		
Ile	N							M	W	M										
	α								M	M										
	β									W										
DhA	N										W									
	βd											S								
	βu												M							
Leu	N													M	W				W	
	α														M					W
Ala$_L$	N															M	W		W	
	α																M	–	M	
	βd																	–		
	βu																			
NMe	N																			M
	Me																			

[a] S, strong; M, medium; W, weak; –, overlap.

Table VIII. Nisin Ring A D-Ala Analog Nuclear Overhauser Effects[a]

		Ac	D-Ala$_L$				Ile				D-Ala			Leu		Ala$_L$				NMe	
		Me	N	α	βd	βu	N	α	γ′		N	α	β	N	α	N	α	βd	βu	N	Me
Ac	Me		M																		
D-Ala$_L$	N			M		W	M										M				
	α				M	M	W														
	βd					S															
	βu						W														
Ile	N							M													
	α								M		S										
	γ′										W										
D-Ala	N											M	W								
	α												S	S							
	β																				
Leu	N													M							
	α															S					
Ala$_L$	N															M		W			
	α																M	M		M	
	βd																		S		
	βu																				
NMe	N																				M
	Me																				

[a] S, strong; M, medium; W, weak; –, overlap.

Table IX. Nisin Ring A L-Ala Analog Nuclear Overhauser Effects[a]

		Ac	D-Ala$_L$				Ile				Ala			Leu		Ala$_L$				NMe	
		Me	N	α	βd	βu	N	α	β	γ′	N	α	β	N	α	N	α	βd	βu	N	Me
Ac	Me		M																		
D-Ala$_L$	N			M		W	M										M				
	α				S	S	W														
	βd					S															
	βu																M	S			
Ile	N							M	W	W	W										
	α								M	S	W										
	β									S	W										
	γ′										W	W									
Ala	N											M	W	W							
	α												S	M							
	β													W							
Leu	N														M						
	α															M					
Ala$_L$	N																M		W		
	α																	M	M	M	
	βd																		S	W	
	βu																				
NMe	N																				M
	Me																				

[a] S, strong; M, medium; W, weak; –, overlap.

determined for Ac-Dha-NHMe in the crystalline environment. Thus, dehydroalanine exerts similar conformational constraints independent of other factors. The Leu[5] residue in this molecule adopts a strained inverse γ-turn orientation as well. An Ala[6]-HN–Dha[4]-O hydrogen bond is suggested by the calculated structure, as well as by the temperature coefficient of the Ala[6] amide.

Conclusion

New parameters have been determined for modeling dehydroalanine which reproduce experimental results from X-ray crystallography and semiempirical quantum mechanical calculations. These parameters generalize to the α-amino-α,β-dehydrobutyric acid residue and may be applicable to modeling other α,β-unsaturated amino acids as well. In the process, we have developed a convenient new approach to parametrizing empirical potential energy functions. These parameters were used in DISCOVER calculations to refine the NMR/distance geometry structure of a cyclic peptide containing dehydroalanine. Dehydroalanine adopted a roughly planar conformation, with trans orientations for the ϕ and ψ torsions, and induced an inverse γ-turn in the preceding residue. Similar effects have been observed for linear dehydroalanine-containing peptides in solution or in the crystalline state, suggesting that dehydroalanine exerts a powerful conformational influence independent of other constraints. This structure differs substantially from structures determined for either D- or L-Ala substituted analogs, which adopt a γ- or inverse γ-turn about the central D- or L-alanine, respectively. We are now investigating whether the pronounced conformational effects of dehydroalanine play a role in the biological acivity of nisin.

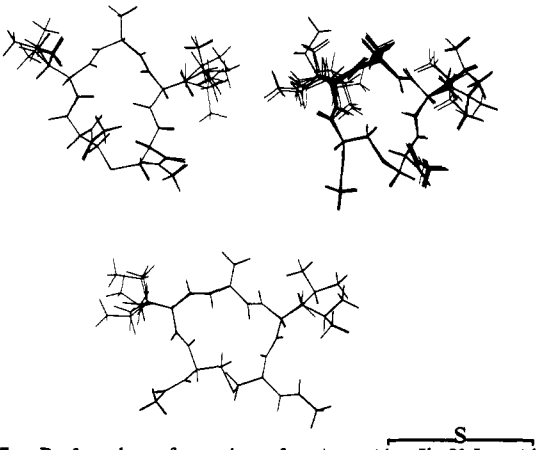

Figure 7. Preferred conformations for Ac-D-Ala$_L$-Ile-X-Leu-Ala$_L$-NHMe in DMSO-d_6, where X = L-Ala (upper left), D-Ala (upper right), or dehydroalanine (lower). These backbone and lanthionine bridge structures were determined through NMR spectroscopy, distance geometry, and conformational energy minimization. The side chain conformations of Ile and Leu were then systematically searched and the structures were reminimized. Whereas the D-Ala and L-Ala analogs exhibit γ or inverse γ-turns about those residues, the dehydroalanine-containing analog processes an inverse γ-turn about the preceding isoleucine.

Acknowledgment. The authors wish to thank John Maple, Anna Tempczyk, Greg Grose, Iouri Bondarenko, Karl Jalkanen, and Arnold Hagler of the Biosym Parameter Consortium for helpful discussions and instruction in their formal procedure for force field parametrization. Adam Winkler provided advice, encouragement, and useful references in the application of simulated annealing. Discussions with Alexander Polinsky, Robert Feinstein, and Anna Toy were also helpful. We acknowledge support of this research through a grant from the National Institutes of Health (GM18694). Most of the calculations presented here were carried out on the San Diego Supercomputer Center's Cray Y-MP computer with a grant of time by the SDSC.

Supplementary Material Available: Structure determination summary and tables of crystallographic parameters, including atomic coordinates, isotropic and anisotropic displacement coefficients, and bond lengths and angles for *N*-acetyldehydroalanine *N*′-methylamide (10 pages); tables of observed and calculated structure factors (7 pages). Ordering information is given on any current masthead page.